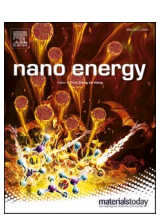
ELSEVIER

Contents lists available at ScienceDirect

Nano Energy

journal homepage: www.elsevier.com/locate/nanoen





A highly-stable layered Fe/Mn-based cathode with ultralow strain for advanced sodium-ion batteries

Rui Qi ^{a,1}, Mihai Chu ^{a,1}, Wenguang Zhao ^a, Ziwei Chen ^a, Lei Liao ^b, Shisheng Zheng ^a, Xiping Chen ^c, Lei Xie ^c, Tongchao Liu ^d, Yang Ren ^e, Lei Jin ^f, Khalil Amine ^{d,g}, Feng Pan ^{a,*}, Yinguo Xiao ^{a,*}

- ^a School of Advanced Materials, Peking University, Shenzhen Graduate School, Shenzhen 518055, China
- ^b Beijing National Laboratory for Condensed Matter Physics, Institute of Physics, Chinese Academy of Sciences, 100190 Beijing, China
- ^c Institute of Nuclear Physics and Chemistry, China Academy of Engineering Physics, Mianyang 621900, China
- ^d Chemical Sciences and Engineering Division, Argonne National Laboratory, Lemont, IL 60439, USA
- ^e X-ray Science Division, Argonne National Laboratory, Lemont, IL 60439, USA
- f Ernst Ruska-Centre for Microscopy and Spectroscopy with Electrons, Forschungszentrum Jülich GmbH, 52425 Jülich, Germany
- ⁸ Material Science and Engineering, Stanford University, Stanford, CA 94305, USA

ARTICLE INFO

Keywords: Sodium-ion battery Fe- and Mn-based layered oxide cathodes Co-substitution strategy Solid-solution reaction Lattice strain

ABSTRACT

Sodium-ion batteries (SIBs) with iron- and manganese-based cathode electrodes have exhibited great promise in the grid-scale energy storage systems, on the basis of the satisfactory theoretical capacity, as well as huge abundance, low price and non-toxicity of raw materials. However, the inferior cycle life of cathode materials originating from their poor structural stability remains a formidable challenge towards practical applications. Here, an efficient strategy of improving the structure durability is demonstrated in iron- and manganese-based cathodes by dual heteroatom doping. The as-obtained P2-type $Na_{0.65}Li_{0.08}Cu_{0.08}Fe_{0.24}Mn_{0.6}O_2$ cathode delivers superior cyclability (88.2% capacity retention for 500 cycles at 2C), fabulous rate capability (76% capacity retention at 5C compared to 0.1C), and a useable reversible capacity of around 85 mAh g⁻¹ at 0.1C. Through indepth characterizations, the underlying structure-property relationship is established, revealing that the complete solid-solution reaction during cycling ensures the ultralow volume variation (as small as 0.7%) and excellent electrochemical performance. These results highlight the significance of fabricating a stable host for the design and development of advanced SIBs with long life.

1. Introduction

Owing to the ever-growing demands for environmentally-benign energy solutions, research and development of large-scale electrical energy storage systems (EESs) for the integration of intermittent renewable energy sources, such as solar, wind and geothermal, is becoming increasingly imperative [1,2]. In this regard, rechargeable sodium-ion battery (SIB) is considered as one of the most attractive options for grid-scale EESs and an alternative to lithium-ion batteries due to the highly abundant and wide distribution of sodium resources compared to lithium [3]. Among the various cathode materials for SIBs, the layered transition-metal oxides (Na_xTMO_2 , $0 < x \le 1$, TM=Ni, Co, Mn, Fe, V, etc.) have been regarded as one of the most promising

candidates for several advantages in terms of their facile synthesis and 2D Na⁺ diffusion pathway [4].

In general, $Na_x TMO_2$ can be classified into two major groups according to the oxygen stacking sequence and local environment of Na^+ , namely P2-type (P: prismatic) and O3-type (O: octahedral) [5]. P2-phase oxides normally exhibit fewer phase transitions and better rate capability in comparison with the corresponding O3-type counterpart on account of their larger prismatic sites and direct diffusion pathways for Na^+ [6]. As a consequence, $P2-Na_{2/3}Fe_{1/2}Mn_{1/2}O_2$ possesses a much more remarkable electrochemical performance than O3-NaFe_{1/2}Mn_{1/2}O₂, delivering a high capacity of 190 mAh·g⁻¹ within the voltage of 1.5–4.3 V [7]. It is also worth noting that both iron and manganese elements are extremely abundant in the earth's crust among

E-mail addresses: panfeng@pkusz.edu.cn (F. Pan), y.xiao@pku.edu.cn (Y. Xiao).

^{*} Corresponding authors.

¹ These authors contributed equally to this work.

all the 3d transition metals [8]. The P2 Na-Fe-Mn-O cathodes obviously demonstrate great potential as commercialized cathodes for SIBs in view of their satisfactory theoretical capacity, low cost in raw materials and environmental benignity [8–11]. However, the practical application of these P2-type Fe- and Mn- based oxides is seriously hindered by their insufficient structural stability during cycling, which is ascribed to the formation of unfavorable P2-Z phase transition at a high-voltage region and the destabilization of the crystal structure associated with Jahn-Teller distortion of Mn $^{3+}$ upon Na $^{+}$ (de)intercalation [12–14]. In addition, P2-type Na $_{\rm x}$ Fe $_{\rm 1-y}$ Mn $_{\rm y}$ O $_{\rm 2}$ materials are hygroscopic, thus resulting in a shorter lifetime and added cost for storage and transportation [15].

To alleviate the aforementioned issues faced by P2-Na_xFe_{1-v}Mn_vO₂, tremendous efforts have been exerted in previous studies, such as heteroatom doping [8,11], surface engineering [16] and nanoscale design [17]. Noticeably, doping various metallic cations (inactive ions: Li⁺ [18, 19], Mg^{2+} [20], Al^{3+} [21], Ti^{4+} [22,23]; active ions: Ni^{2+} [24], Co^{3+} [25,26], Cu²⁺ [27,28]) is commonly recognized to be an effective way to improve their performance. For example, Ni and Co were introduced to transition metal layers to fabricate the trinary Ni/Fe/Mn- and Co/Fe/Mn- based oxides respectively, showing an improved performance to some extent by relieving the phase transition and structural distortion [25,29]. Considering the relatively expensive price of Ni and Co, a Cu-substituted P2-Na_{7/9}Cu_{2/9}Fe_{1/9}Mn_{2/3}O₂ was synthesized. This material exhibited a reversible capacity of 89 mAh·g⁻¹ at 0.1C and a complete solid-solution reaction with good capacity retention (85% after 150 cycles at 1C) [30]. Nonetheless, it is still not competent to achieve ultra-long-term cycles in P2-type Fe- and Mn- based cathodes. It should be demonstrated that for grid-scale EESs, low production cost and superior cycling stability are critically important [31]. Besides, for P2-type Fe- and Mn- based oxides, impurities are inclined to produce without suitable compositions and substituents/dopants [32]. Therefore, it is urgent to explore novel Ni/Co free cathodes with excellent calendar life and high tolerance toward moisture through a scalable

Herein, Li/Cu co-substitution is proposed to improve the practicality of P2-Na_xFe_{1-v}Mn_vO₂, since dual heteroatom doping strategy could not only combine different merits of dopants but boost the concentration of heteroatoms in materials [33]. For example, some quaternary, quinary and even high entropy layered oxide cathodes enabled by doping two or more metallic elements commonly delivered good energy storage properties [34–36]. Nevertheless, to the best of our knowledge, the heteroatom co-doping method has rarely been adopted for the P2-type Fe- and Mn- based system. Among all of the dopant cations, Li substitution in the TM layer is considered as structure stabilizer because the monovalent Li⁺ is beneficial to keep more Na⁺ retain in the deeply desodiated structure to maintain electrostatic equilibrium [37]. Consequently, suppressed phase transitions (i.e., P2-O2, P3-P'3) and smooth charge-discharge curves were reported in Li-substituted Na_xTMO₂ cathodes [38-40]. Meanwhile, the Cu-doped oxides were developed, including P2-Na_{0.67}Cu_{0.33}Mn_{0.67}O₂ [41], P2@P3 Na_{0.78}Cu_{0.27}Zn_{0.06} $Mn_{0.67}O_2$ [42], etc., in which the reversible Cu^{2+}/Cu^{3+} redox is responsible for the improved working potential and air stability.

Enlighted by the above considerations, a quaternary P2-type $Na_{0.65}Li_{0.08}Cu_{0.08}Fe_{0.24}Mn_{0.6}O_2$ (NLCFM) was successfully designed for the first time via Li/Cu co-substitution. As a comparison, the electrochemical performance of undoped P2- $Na_{0.65}Fe_{0.4}Mn_{0.6}O_2$ (NFM), monodoped P2- $Na_{0.65}Li_{0.08}Fe_{0.32}Mn_{0.6}O_2$ (NLFM) and P2- $Na_{0.65}Cu_{0.08}Fe_{0.32}Mn_{0.6}O_2$ (NCFM) were systematically investigated, and their phase structures were confirmed by neutron diffraction coupled with X-ray diffraction. For the P2-NLCFM electrode, in-situ synchrotron high-energy X-ray diffraction (HEXRD) reveals that the unwanted P2-Z phase transition has been strongly mitigated during the charge/discharge process with the unit cell volume variation as small as about 0.7%. As a consequence, outstanding structural stability and greatly enhanced rate capability were achieved. The Li/Cu co-doping NLCFM

cathode exhibits a specific capacity of around 85 mAh·g⁻¹ at 0.1C between 2.5 and 4.2 V with a high average voltage of 3.5 V and ultrastable cycle performance (88.2% capacity retention at 2C after 500 cycles). The ex-situ XRD experiments, high-resolution transmission microscopy (HRTEM), galvanostatic intermittent titration technique (GITT) and differential electrochemical mass spectrometry (DEMS) were further conducted to investigate the linkage between electrochemical performance and structure durability, and demonstrated the significance of a stable host for Na⁺ insertion/extraction.

2. Experimental section

2.1. Materials synthesis

 $Na_{0.65}Fe_{0.4}Mn_{0.6}O_2$ (NFM), $Na_{0.65}Li_{0.08}Fe_{0.32}Mn_{0.6}O_2$ (NLFM), $Na_{0.65}Cu_{0.08}Fe_{0.32}Mn_{0.6}O_2$ (NCFM) and $Na_{0.65}Li_{0.08}Cu_{0.08}Fe_{0.24}Mn_{0.6}O_2$ (NLCFM) were prepared by a conventional solid-state reaction from the precursor of Na₂CO₃ (Sinopharm Chemical, 99.8%), Fe₂O₃ (Aladdin, 99.9%), Li₂CO₃ (Sinopharm Chemical, 99.99%), CuO (Sinopharm Chemical, 99%), and Mn₂O₃ (98%, Sinopharm Chemical). For Na_{0.65}Fe_{0.4}Mn_{0.6}O₂, Na₂CO₃, Fe₂O₃, and Mn₂O₃ were mixed together with a molar ratio of 0.67:0.4:0.6 (3% excess Na₂CO₃ to compensate for the volatilization loss at high temperatures) and thoroughly ground by a ball mill at 400r min⁻¹ for 6 h. The resulting mixture was pressed into pellets under the pressure of 20Mpa. Then, the pellets were calcined at 900 °C for 15 h in O2. After cooling down naturally, the sample was transferred to an Ar-filled glovebox immediately until use. The synthesis procedure of doped samples, NLCFM, NLFM and NCFM followed the identical procedure via mixing the relevant oxide in a stoichiometric ratio.

2.2. Materials characterizations

The composition of the final materials was detected by inductively coupled plasma-atomic emission spectrometry (ICP-AES, JY2000-2, HORIBA JOBINYVON). The crystalline structures of the samples were investigated by both X-ray and neutron diffraction measurements. The X-ray diffraction (XRD) patterns were collected on a Bruker D8 Discover diffractometer with Cu K α radiation of $\lambda=1.5405(6)$ Å within the 2θ range of 10-80°. Neutron powder diffraction (NPD) experiments were performed at room temperature on the High-Pressure Neutron Diffractometer (HPND) at China Mianyang Research Reactor (CMRR). Roomtemperature data were collected at a wavelength of $\lambda = 1.5907(1)$ Å. Rietveld refinement of the diffraction profiles was carried out using the FullProf package suite. In addition, the particle morphology and elements distribution were examined using a scanning electron microscope (SEM, ZEISS SUPRA-55) with an Energy Dispersive Spectroscopy (EDS, OXFORD, X-MaxN TSR) and all these cross-section samples were prepared by focused ion beam (FIB, FEI, Scios). High-resolution transmission electron microscopy (HRTEM) images were obtained on a JEOL-3200FS field-emission transmission electron microscopy (FETEM) with 300 kV accelerating voltage. To observe the oxidation states of the transition metal elements, electron energy loss spectroscopy (EELS) data were collected using a 300KV aberration-collected STEM (JEM-ARM300F, JEOL Ltd). X-ray photoelectron spectra (XPS) was performed by a Thermo Fisher ESCALAB 250X using a monochromatic Al Kα X-ray source, and all the binding energy were calibrated with C 1s signal at 284.8 eV. Especially for the ex-situ EELS, XPS and XRD measurements, the post cycled electrodes were first transferred to a hermetically sealed transfer chamber in a glovebox filling with Ar to prevent exposure to air or moisture. As for in-situ XRD studies, the time-resolved HEXRD experiment was performed on NLCFM material during the first cycling at beamline 11-ID-C, Advanced Photon Source (APS), Argonne National Laboratory (ANL), with the wavelength of 0.1173 Å. The NLCFM cathode electrode was prepared using PVDF as binder on an ultrathin Al foil and the diffraction patterns were collected every 10 min in a 2θ range of 0° — 4° under cycling. Moreover, DEMS experiments were carried out in a customized cell connected to a gas flow controller and mass spectrometer by using Agilent Technologies 5975C.

2.3. Electrochemical measurements

The cathode electrodes were prepared by using the following steps. As-prepared active materials were mixed with acetylene black and poly (vinylidene fluoride) (PVDF) with a weight ratio of 8:1:1 in N-methyl-2pyrrolidone (NMP). After stirring for 6 h, the homogeneous slurry was spread on the clean Al foil, followed by drying at 110 °C in a vacuum oven overnight. Metallic Sodium disk was employed as the counter electrode and glass fiber was used as the separator. The electrolyte was a solution of 1 M NaClO₄ in ethylene carbonate/diethyl carbonate (EC/ DEC,1:1 in volume) with fluoroethylene carbonate (FEC 5% in volume) as additive. The assembly of the CR2032-type coin cells was carried out in an Ar-filled glove box. Galvanostatic discharge/charge tests were performed using a NEWARE battery cycler at room temperature. In the ultra-long cycling test, one formation cycle was performed at 0.1C, followed by cycling at 2 C. GITT measurement was carried out on a Maccor test cabinet in the voltage range of 2.5–4.2 V vs Na⁺/Na. The Cyclic voltammogram curves were tested by the CHI660D electrochemical workstation (CHI Instruments, China).

3. Results and discussion

3.1. Structure and chemical composition analysis

To prove the effectiveness of the Li/Cu co-substitution, the target samples NFM and NLCFM, as well as mono-doped samples, were synthesized by a solid-state method. ICP-AES measurement results indicate that the chemical formulas of as-prepared materials are consistent with the expected stoichiometry (Table S1). To obtain the accurate lattice parameters and precise atomic positions, the joint refinements based on both XRD and NPD profiles were performed. As X-ray alone is not sensitive to light elements such as Li and could hardly distinguish elements with similar atomic numbers such as Fe and Mn, neutron could make up

for that with the advantage of the sensitivity against nuclei of all atoms involved. As shown in Fig. 1 and Fig. S1, the Rietveld refined NPD and XRD patterns demonstrate that all Bragg reflections in each individual sample, as expected, could be assigned to the P2-type layered structure (space group: P63/mmc, JCPDF no. 27-751) without any impurity. The good agreement between the fitting and experiment patterns confirms that Li, Cu, Fe and Mn atoms are all located in the TM layer (Fig. 1c and f). Additionally, there is no noticeable reflection corresponding to longrange in-plane ordering associated with TM ion units or Na⁺/vacancy ordering. The detailed structural information is given in Table S2. A slight lattice contraction was observed with the introduction of Li and Cu, where a=2.9224(1) Å and c=11.2336(3) Å for NFM and a = 2.9028(1) Å and c = 11.1469(3) Å for NLCFM. This contraction was caused by the oxidation of the Mn^{3+} to Mn^{4+} (ionic radii of Mn^{3+} is larger than that of Mn⁴⁺) due to the presence of the Li⁺ and Cu²⁺ in the TM layer. In addition, after co-doping, the thickness of Na layer (T_{Na}) decreases while the thickness of TM layers (T_{TM}) increases.

The HRTEM images in Fig. S2 further corroborate the typical P2 structure of all four samples, where the (002) plane and the fast Fourier transform (FFT) images (inset of Fig. S2) are clearly shown. However, for the samples containing the single dopant element, when their anticipated content of heteroatom was raised to the same amount in NLCFM ($Na_{0.65}Li_{0.08}Cu_{0.08}Fe_{0.24}Mn_{0.6}O_2$), the expected stoichiometry $(Na_{0.65}Li_{0.16}Fe_{0.24}Mn_{0.6}O_{2-x}, Na_{0.65}Cu_{0.16}Fe_{0.24}Mn_{0.6}O_{2})$ could not be achieved and the impurities would arise (Fig. S3), implying the cosubstitution strategy is beneficial to boost the content of heteroatoms in materials [33]. In addition, SEM images show that all samples exhibit plate-like particles with around 2–4 µm in size (Fig. S4). EDS mapping images reveal that various elements uniformly distribute throughout particles without any aggregation (Fig. S5). All the above results confirm the target cathodes are successfully prepared and heteroatom-doping strategy has negligible influence on sample morphology and element distribution, laying the groundwork for further investigating their performance and behaviors.

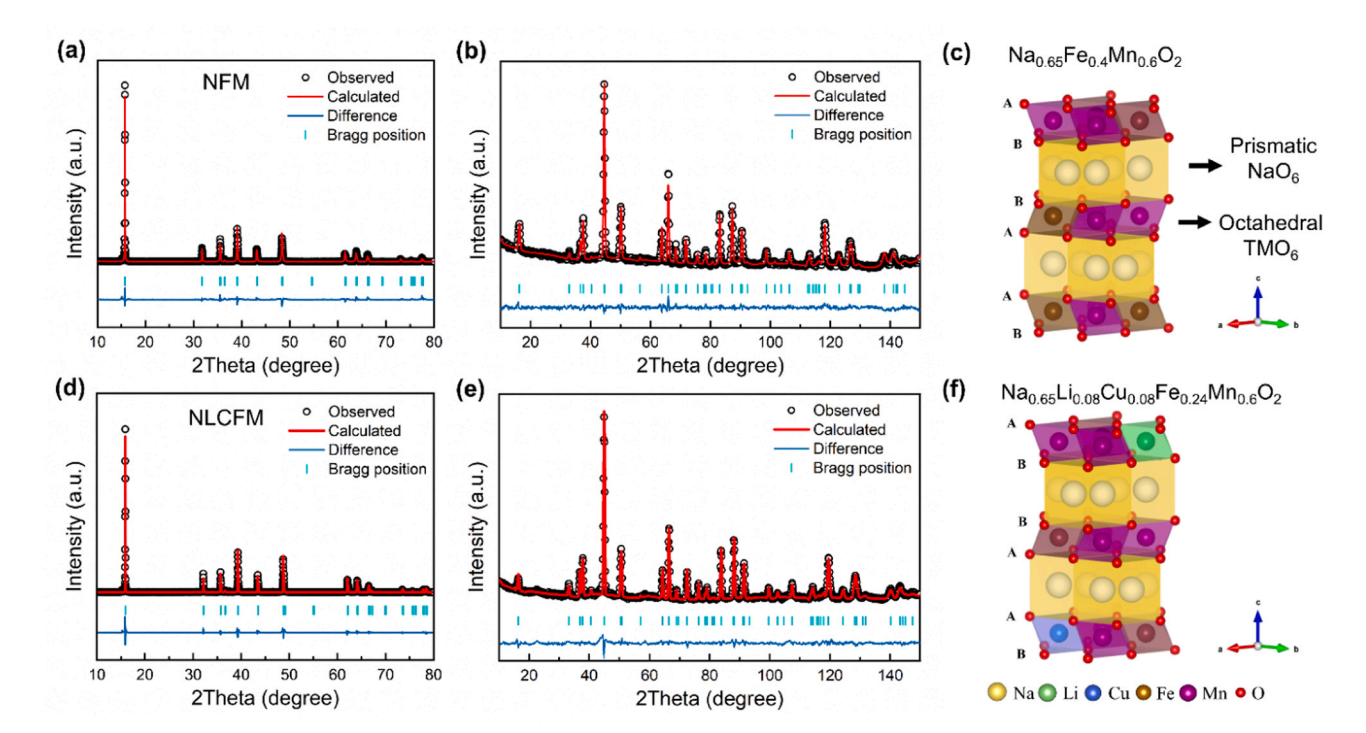


Fig. 1. Crystal structure characterization on powder samples of NFM and NLCFM. (a–b, d–e) Observed and calculated XRD and NPD profiles for NFM and NLCFM. (black) observed; (red) calculated; (blue) difference plot; (green bars) Bragg reflections. (c, f) Schematic illustration of the crystal structure of NFM and NLCFM.

3.2. Electrochemical behavior

The electrochemical performances of the NFM and NLCFM were comparatively studied in sodium half cells. Fig. 2a and b show the galvanostatic charge/discharge curves in a voltage range of 2.5-4.2 V at a current rate of 0.1 C (10 mA g⁻¹). In the first cycle, NFM electrode delivers a discharge specific capacity of 100 mA h g⁻¹ and two distinct voltage plateaus at 4.1 V and 3.5 V are observed, corresponding to phase transitions [14]. A much lower discharge capacity of 85 mA h g⁻¹ is left just after 10 cycles accompanied by the shortening of the voltage plateaus, in accordance with the rapid decay of two obvious peaks in the dQ/dV curves (Fig. 2d), revealing that severe irreversible behaviors occur during the cycling. In contrast, NLCFM electrode proceeds through a more solid-solution like reaction (Fig. 2b), as reflected in sloping charge/discharge profiles as well as highly reversible dQ/dV curves (Fig. 2e). Interestingly, the specific capacity of NLCFM gradually increases from 78 mA h g⁻¹ to 85 mA h g⁻¹ during the initial 10 cycles, and even reaches 90 mA h g⁻¹ after 40 cycles (Fig. 2c), which could be attributed to the minimization of Mn³⁺ content after Li/Cu co-substitution and consequent gradual electrochemical activation of Mn³⁺/Mn⁴⁺. Their performance differences are clearly demonstrated in Fig. 2c. With the increasing cycle number at 0.1C, the NFM electrode encounters very fast capacity decay with an inferior retention of only 40% after 100 cycles, while NLCFM exhibits great superiority in both cyclability and average potential. Moreover, the GITT result in Figs. 2f and S6 indicates that Na-diffusion coefficients (D_{Na}) in NFM exhibits a sharp drop at around 3.5 V during the initial discharging, corresponding

well to the plateau shown in discharge profile (Fig. 2a). The occurrence of minima signals the attenuation of Na⁺ mobility, which could be attributed to the host rearrangement [43]. All these results preliminarily demonstrate the feasibility and effectiveness of our heteroatom co-doping strategy, in which the introduction of Li/Cu as heteroatoms is greatly in favor of the cycling performance, midpoint voltage and rate capability of cathodes.

In order to clarify the role of each heteroatom in the co-substitution NLCFM sample, four as-prepared electrodes including mono-doped ones were tested by CV between 2.5 and 4.2 V, shown in Fig. S7. In pristine electrode, the anodic peaks at potentials higher than 3.9 V, as well as the cathodic peak at around 3.5 V, are attributed to the redox reactions of the Fe³⁺/Fe⁴⁺ couple, while the peaks below 2.7 V should correspond to the redox reactions of the Mn³⁺/Mn⁴⁺ [24]. With the Cu-substitution, the abovementioned anodic peak of Fe³⁺/Fe⁴⁺ becomes broader due to the incorporation of oxidation/reduction peaks of Cu²⁺/Cu³⁺ (4.0/3.9 V) [28], which could contribute to the capacity and improve the working potential in the electrode. With the Li-substitution, the smoothing of peaks in NLFM are achieved and the CV profiles in the first 5 cycles have better overlapping compared to the NFM and NCFM, suggesting optimized structural reversibility during cycling. In the case of Li/Cu co-substitution, the disappearance of Mn³⁺/Mn⁴⁺ redox peaks induced by maximization of Mn4+ content, and the mergence of Fe³⁺/Fe⁴⁺ and Cu²⁺/Cu³⁺ redox peaks [28,30], jointly lead to more sloping and flat CV curves, indicating that the structure of NLCFM is stable upon Na+ insertion/extraction. In addition, as elucidated in Figs. S8 and S9, these redox activities are detected by XPS and EELS.

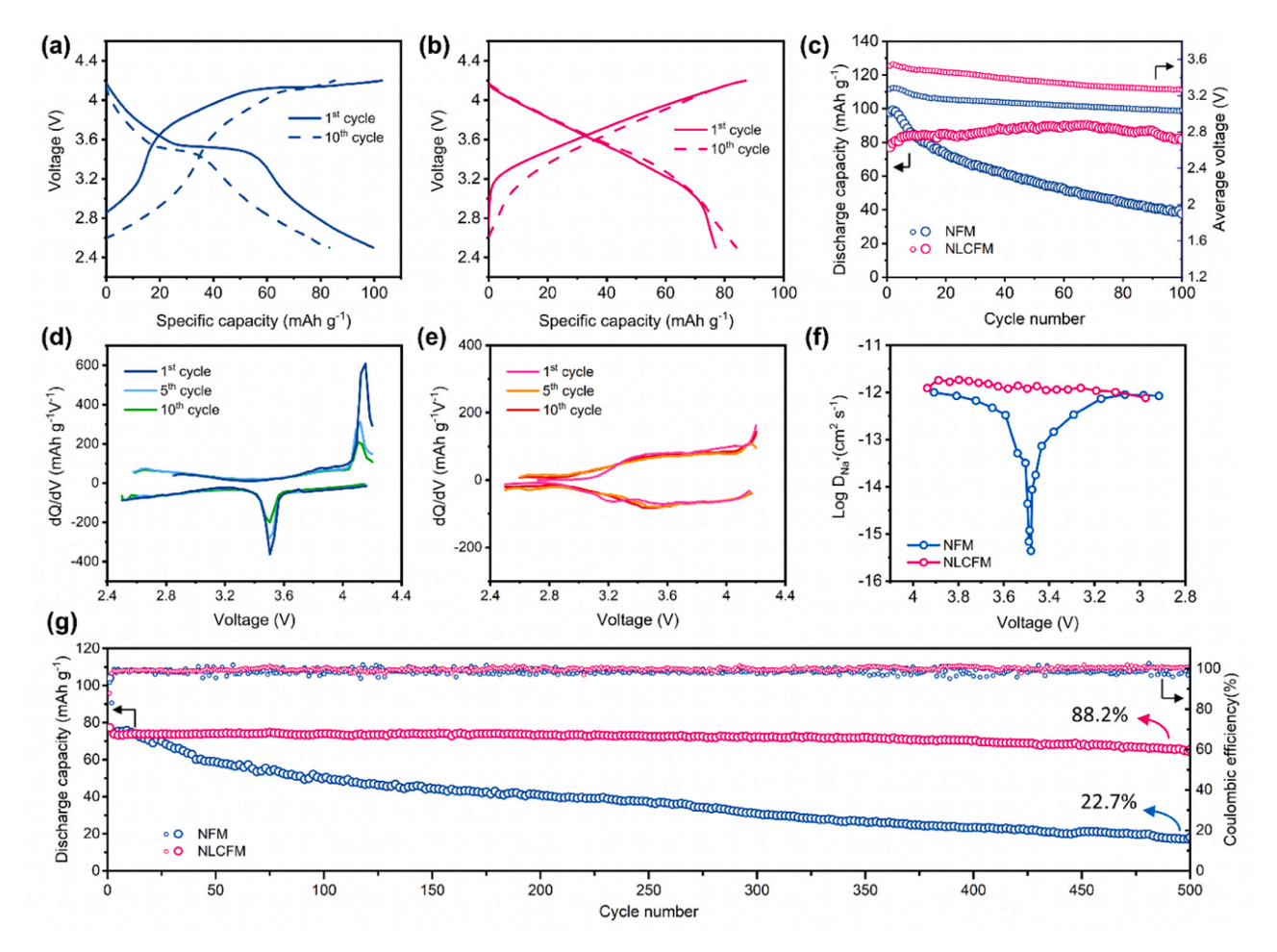


Fig. 2. Electrochemical performance of NFM and NLCFM electrodes in half-cell system. (a–b) Galvanostatic charge/discharge curves at 0.1C of NFM and NLCFM electrodes, respectively. (c) Comparisons of average voltage and cycling performance at 0.1C. (d–e) dQ/dV curves of NFM and NLCFM electrodes. (f) Na⁺ chemical diffusion coefficient calculated from GITT data for NFM and NLCFM electrodes. (g) Cycling performance of NFM and NLCFM at 2C over 500 cycles.

Therefore, upon initially charging to 4.2 V, a charge capacity of 102.8 mAh $\rm g^{-1}$ is achieved through the directly oxidation of $\rm Mn^{3+}$ and $\rm Fe^{3+}$ in NFM, corresponding to 0.39 Na⁺ extraction from the host. As for NLCFM, the first charging capacity matches well with its theoretical capacity, in which 0.32 Na⁺ are removed, and the $\rm Cu^{2+}/\rm Cu^{3+}$ and $\rm Fe^{3+}/\rm Fe^{4+}$ redox couple contribute to almost all the experimental capacity.

Given the results of the rate and cycling performance of these four electrodes in Fig. S10, it further confirms that Cu contributes to the capacity and Li improves the stability. With the help of these two kinds of heteroatom substitution, the NLCFM exhibits the best rate capability and cycling stability among four kinds of Fe- and Mn- based oxides. Therefore, a longer cycling test of NLCFM was conducted at 2C and it exhibits outstanding cycling performance, as shown in Fig. 2g. A capacity retention of 88.2% is achieved after 500 cycles, with the capacity loss rate of only about 0.026% per cycle, corroborating the superior reversibility during cycling.

3.3. Structural evolution of electrodes upon Na⁺ (de)intercalation

To understand the nature of discrepancies in electrochemical performance, the structural evolutions of the NFM and NLCFM electrodes during the first cycle were analyzed by ex-situ XRD (Fig. 3). Seven key points indicated by colored circles were selected, and corresponding XRD patterns of NFM are shown in Fig. 3a. It is clear that the phase transformation occurs when the NFM electrode crosses the long plateau at around 4.1 V and 3.5 V, respectively, in accordance with the low $D_{\rm Na}^+$ deduced from GITT results. When the NFM electrode is charged to 4.1 V, the intensity of P2 (002) peak at $2\theta=15.8^\circ$ decreases dramatically along with the emergence of a new characteristic peak at its right side. Combined with other reflections, this newly formed phase is assigned to

the "Z" phase with low crystallinity [7,12]. Upon further charging, this new characteristic reflection gradually reached $2\theta = 17.1^{\circ}$ and the "Z" phase almost dominated the structure. The peaks indexed in "Z" phase are weak and broad, indicating an evolving intergrowth between the P-type stacking (Na in prismatic sites) and O-type stacking (Na in octahedral sites) [44]. During the discharge process, the P2 reflections reappear at around 3.5 V at the expense of the "Z" phase. The evolution of the lattice parameters determined by Le Bail fitting methods could also demonstrate the phase transition. As presented in Fig. 3b, the in-plane lattice parameter experiences an evident decrease from 2.91 Å to 2.85 Å upon desodiation process. Meanwhile, the average interlayer distance of NFM undergoes a sharp contraction from 5.63 Å to 5.20 Å because the interlayer spacing of newly formed O-type layers induced by the glide of TMO₂ slabs at high voltage is much smaller than the original P-type layers [45], as illustrated in Fig. S11. Although all these lattice parameters nearly return to their initial values at the end of discharge, suggesting a reversible P2-Z phase transition, the huge lattice variations were still clearly observed in the NFM electrode.

Very different from the NFM electrode, the XRD patterns for NLCFM in Fig. 3c show no new peaks beyond the P2 phase during the entire charge and discharge process. The complete solid-solution reaction is also reflected in the continuous change of the in-plane lattice parameter and the average interlayer distance (Fig. 3d). Note that the colorhighlighted regions representing the range of parameters evolution in the NFM electrode (1.79% along a-axis and 7.68% along c-axis) is much larger than that in the NLCFM electrode (0.78% along a-axis and 1.12% along c-axis). It is also worth noting that, even with the same amount of Na⁺ extraction/insertion, NLCFM always exhibits slighter changes in cell parameters compared with the NFM electrode. The obvious difference in structural characteristics between two samples lead to different electrochemical behaviors, indicating that the suppression of P2-Z host

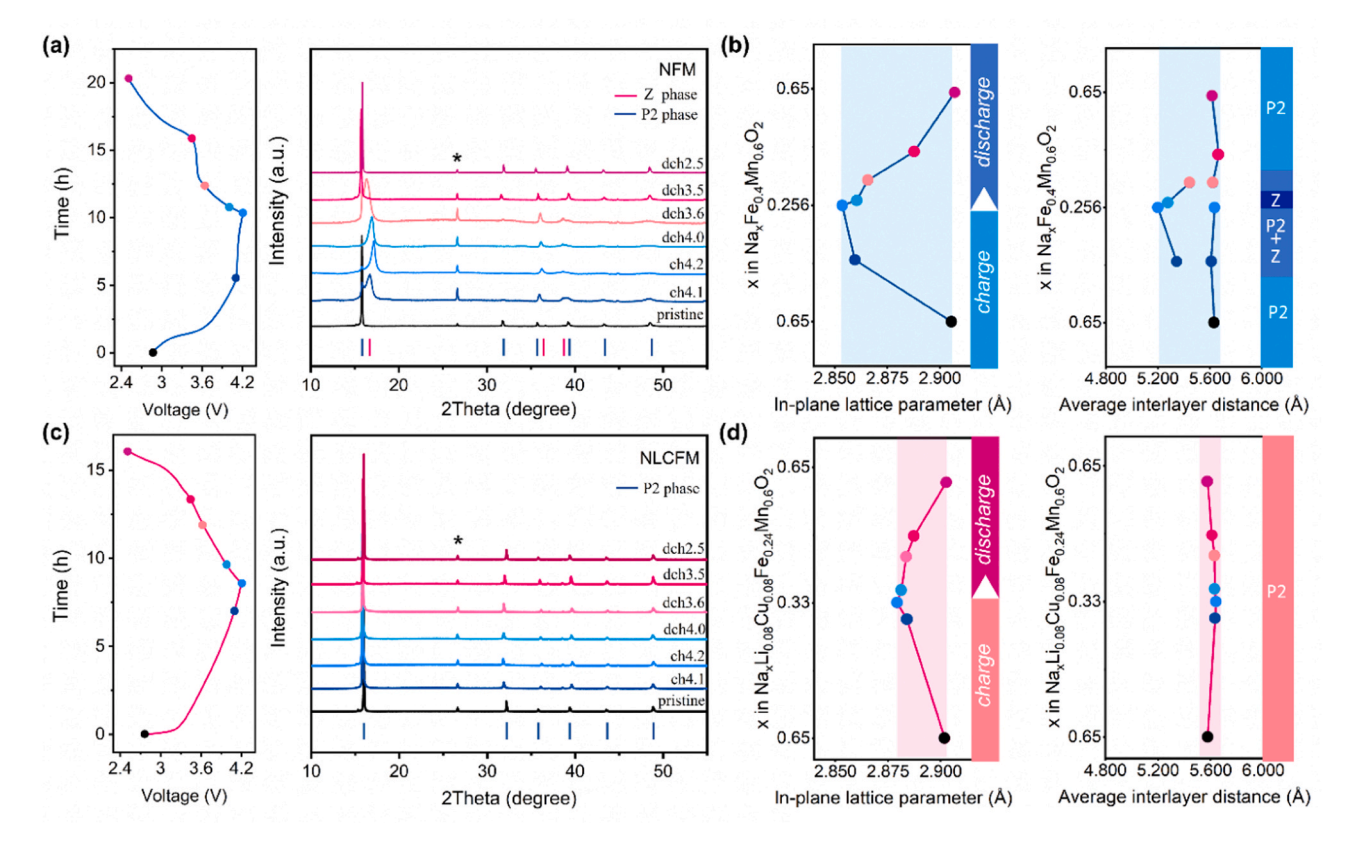


Fig. 3. Ex-situ XRD characterization on the structural evolution of NFM and NLCFM electrodes. (a, c) The ex-situ XRD patterns were collected during the first cycle under a current rate of 0.1 C for NFM and NLCFM electrodes, with the corresponding first cycle electrochemical curves on the left. * represents the peaks from Al foil. (b, d) The evolution of in-plane lattice parameter, average interlayer distance fitted by ex-situ XRD patterns.

rearrangement should account for the improved rate capability and cycling life. Further inspections on the XRD patterns of the mono-doped samples at the fully charged state (Fig. S12) also demonstrate a similar phenomenon, in reasonable agreement with their performance (Fig. S10).

For the NLCFM electrode, the single-phase solid-solution reaction with good reversibility is further confirmed by the in-situ HEXRD results (Fig. 4). Specifically, during the first charge, the (002) peak gradually shift leftward, while (100) and (101) peaks shift rightward, demonstrating the enlarged electrostatic repulsion between adjacent oxygen layers and electrochemical oxidation of TM ions respectively. Consequently, when Na⁺ is extracted, nearly linear contraction of the in-plane lattice (0.93% along a-axis) and expansion of interlayer distance (1.19% $\,$ along c-axis) were precisely monitored, showing a similar tendency with ex-situ XRD results. Not only could NLCFM electrode recover to pristine state regarding all the diffraction peaks and lattice parameters upon discharge, but it experiences an ultralow cell volume change of around 0.7% during the whole cycle. The nearly "zero strain" [46-48] performance represents the minimum value for the Li-doped P2 Fe/Mn-based and Cu-doped P2 Fe/Mn-based layered oxide cathodes for SIBs to date (Table S3). In short, ex-situ XRD and in-situ HEXRD corroboratively confirm that Li/Cu co-substitution for P2-type Fe- and Mn- based oxides can effectively prevent P2-Z phase transition and restrain the volume changes simultaneously during cycling, enabling the zero-strain characteristic and excellent electrochemical properties. In addition, to illustrate the zero-strain characteristic better, the lattice variation of some previously reported cathodes is also reviewed in Fig. S13.

3.4. Failure analysis of electrodes

In order to gain more insight into the differences between two materials in electrochemical reversibility, both of the electrodes after 50 cycles were subjected to post-mortem analysis. As shown in Fig. 5a, after cycling, a mass of cracks could be observed in the cross-sectional image of the NFM sample at low magnification. However, the NLCFM particle is almost intact and only a few tiny microcracks appear. At high magnification, the HRTEM patterns (Fig. 5b-c) acquired along the [100] axis show that distinct cracking and severe local structural distortion occurred in the bulk and surface region of the post cycled NFM, contrasting to the well-maintained (002) layered planes in Li/Cu cosubstitution electrode. From these results, we found that the structural integrity of NFM and NLCFM are well in accordance with the cycling stability plots displayed in Fig. 2, in which the NFM suffers rapid capacity fade while the NLCFM sample possesses extraordinary cyclability. It is also intriguing to note that the intragranular cracks (highlighted by dashed blue lines in Fig. 5b) exhibit evident crystallographic orientation, which is parallel to the (002) planes and consistent with the direction of Na⁺ shuttling. Notably, similar intragranular cracking, which generally appears near the charging end with phase transition, has also been reported in other layered oxide cathodes for Na- and Li-ion batteries [49–52]. Therefore, combined with lattice parameter changes displayed in Fig. 3, cracks on the NFM particle can be correlated to the

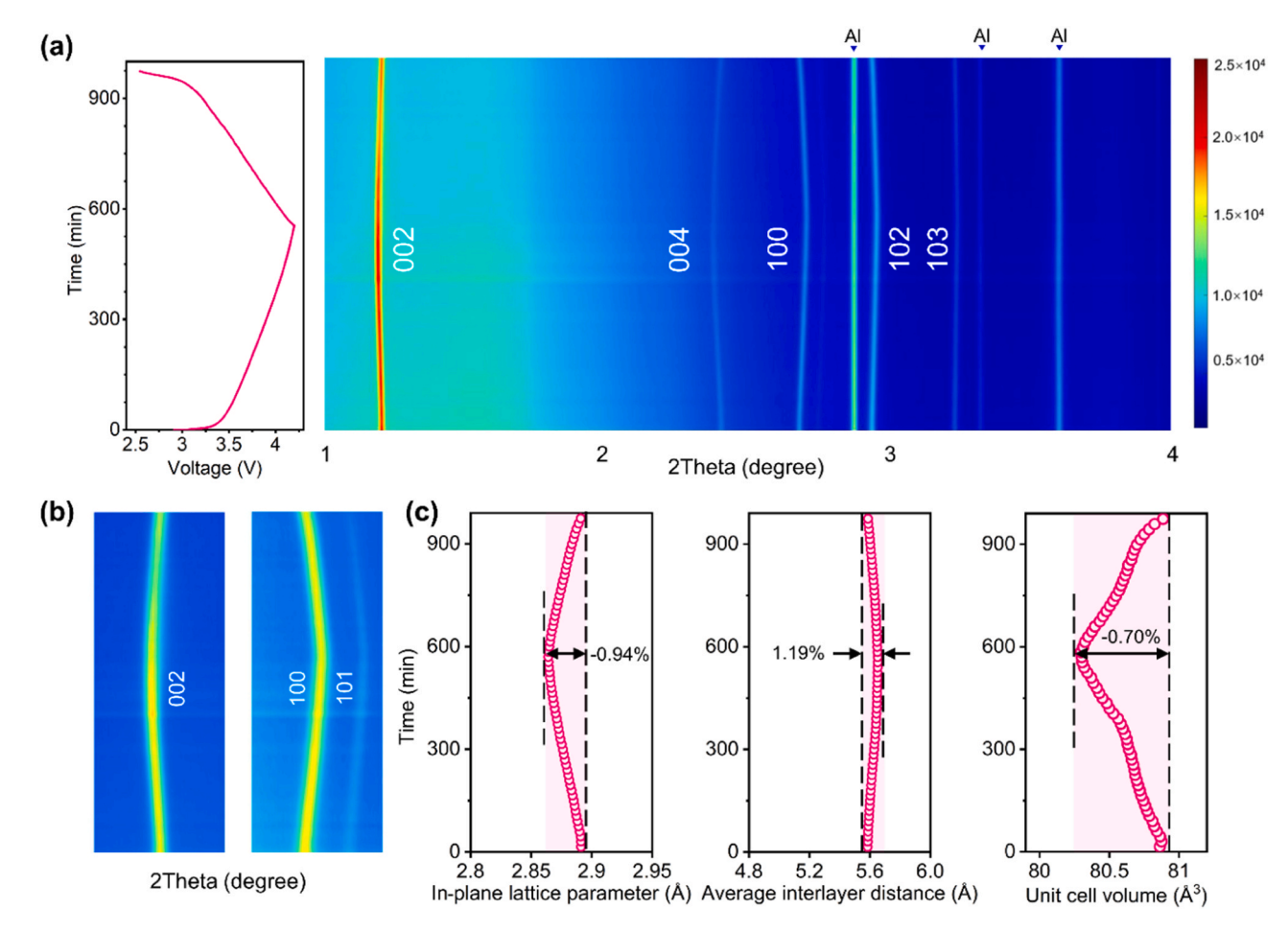


Fig. 4. In-situ synchrotron HEXRD characterization on the structural evolution of NLCFM electrode. (a) The contour plot of in-situ XRD patterns collected under a current rate of 0.1C, with the corresponding first cycle electrochemical curves on the left. (b)Processed images of Bragg peaks (002), (100) and (101) for NLCFM. (c) The evolution of in-plane lattice parameter, average interlayer distance and unit cell volume for the NLCFM electrode fitted by in-situ synchrotron XRD patterns.

R. Qi et al. Nano Energy 88 (2021) 106206

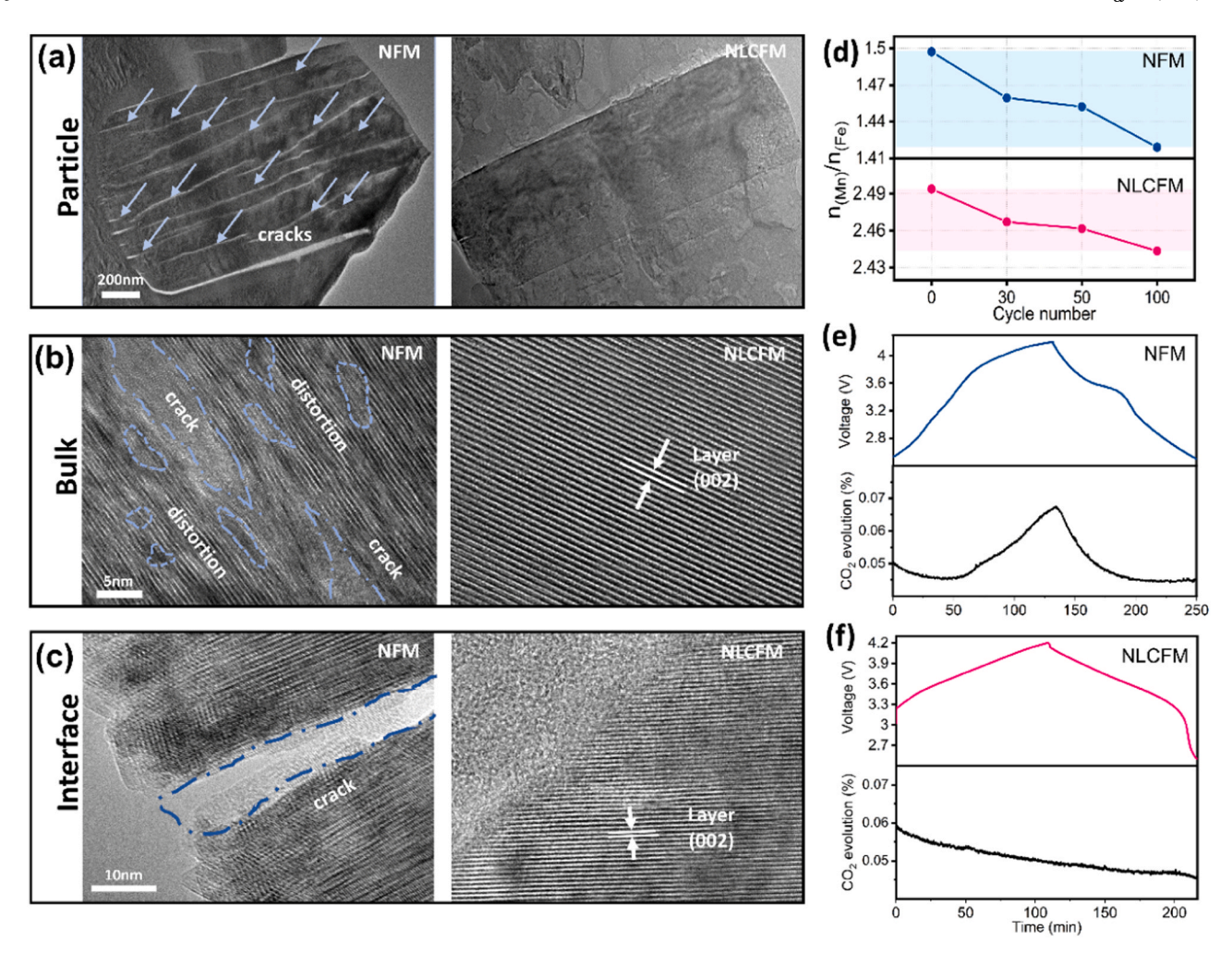


Fig. 5. Post-mortem analyses of NFM and NLCFM electrodes. (a) The cross-sectional images of the particles at low magnification. (b–c) The HRTEM images acquired in the bulk and at the interface. (d) The trend in the molar ratio of Mn to Fe within cathode electrodes during cycling. (e–f) CO₂ evolution of NFM and NLCFM cathodes upon first cycle.

huge internal lattice stress caused by the deleterious P2-Z phase transition. Besides, with prolonged cycling, it is quite possible that the highly distorted lattice area shown in Fig. 5b finally will evolve into cracking region.

In terms of the outermost section of cathodes particle (Fig. 5c), a thick degraded surface layer without the original ordered P2 lattice structure appeared in the NFM sample, which could be attributed to detrimental side reactions on the electrolyte-cathode interphase [53], including TM dissolution, electrolyte decomposition, etc. Particularly for the Mn-rich cathodes, Mn dissolution has been proven to be highly associated with surface degradation because of the destructive Jahn-Teller distortion and disproportionation of Mn³⁺ [54]. To verify this point, ICP-AES was employed to investigate the degrees of Mn dissolution from electrodes at different cycle rates. According to the profile in Fig. 5d, though both NFM and NLCFM electrodes show a decreasing trend in the mole ratio of Mn to Fe during half-cell cycling, the figure for NLCFM still exhibits fewer changes than NFM with the identical cycle period. By the end of 100 cycles, the figure for n(Mn)/n (Fe) has dropped from around 1.5 to below 1.42 in NFMO, while that of NLCFM decreased from nearly 2.5 to over 2.44, maintaining comparatively stable. Besides, based on previous findings, Mn is more susceptible to the attack of HF and solvent molecules than Fe [39]. Hence, the above results clearly suggest that Mn dissolution in NLCFM is far less than NFM. This phenomenon could probably be explained by the

minimization of the quantity of Mn^{3+} in NLCFM through Li/Cu co-substitution, which leads to low Mn³⁺/Mn⁴⁺ redox activity (Fig. S8, 9), a corresponding decrease in Jahn-Teller distortion, disproportionation behavior, and consequent Mn dissolution [55,56]. Meanwhile, as previously studied, the scavenging effect of Li dopant could also help to inhibit the TM cations dissolution and improve the interfacial stability [39]. Moreover, gas evolution, as another byproduct of the parasitic reactions (e.g., decomposition of the residual Na₂CO₃, electrolyte oxidation) on the cathode surface [57], was monitored by DEMS in the initial operation for the NFM and NLCFM cells. In Fig. 5e-f, the volume fraction of CO₂ evolution is plotted as a function of time. As a striking comparison, the CO₂ occurred at around 3.5 V and peaked at the end of charging in the NFM cell, while there is no evidence of CO₂ release in the NLCFM cell, indicating a stable and clean electrode/electrolyte interface has been built for NLCFM, in keeping with the negligible surface structure collapse in NLCFM (Fig. 5c). All the above analyses clearly demonstrate that the repeated P2-Z phase transition with huge lattice strain directly induces cracking generation and particle disintegration, while both TM dissolution and interfacial side reactions contribute to severe capacity decay as well. In addition, during the following cycling, crack propagation and growth would inevitably result in more newly formed surfaces, and thus further accelerating electrolyte consumption, surface degradation, and resultant performance deterioration [50,58].

To further evaluate the application prospects of materials, the NFM

and NLCFM powders were either exposed to air or soaked into water, and then analyzed by XRD. As shown in Fig. S14, after aging experiments, the hydrated layered phase arises apparently in NFM samples, while the NLCFM powders show consistent XRD patterns compared with the pristine one. The excellent air-stability for NLCFM is attributable to the decreased distance of Na layers (Table. S2) and enhanced electrochemical redox potential (diluting redox couple of $\rm Mn^{3+}/\rm Mn^{4+}$ and introducing $\rm Cu^{2+}/\rm Cu^{3+})$ [59,60], which help to suppress the tendency toward $\rm Na^{+}$ extraction and $\rm H_{2}O$ molecule insertion simultaneously.

4. Conclusion

In summary, a novel cathode material Na_{0.65}Li_{0.08}Cu_{0.08}-Fe_{0.24}Mn_{0.6}O₂ for sodium-ion battery was designed and synthesized successfully, based on the Li/Cu co-substitution strategy of combining the strengths of different heteroatoms. It is confirmed the introduction of lithium and copper raises the average redox potential and stabilizes the lattice structure simultaneously. As a result, high average voltage of ~3.5 V, high tolerance toward moisture, and the excellent cycle stability (88.2% capacity retention after 500 cycles) are achieved, suggesting an extremely promising cathode material. Combing with in-situ and ex-situ XRD characterizations as well as detailed post-mortem analysis, we revealed that stable host with less TM dissolution and negligible accumulated strains (unit cell volume evolution as low as 0.7%) upon cycling is the key to deliver outstanding electrochemical performance. For the co-substituted electrode, the P2-Z phase transition is completely suppressed within the voltage range of 2.5-4.2 V, so achieving a solidsolution-like reaction and excellent cyclability. Such a universal cosubstitution strategy could also be employed to other intercalation cathodes. Moreover, our findings demonstrate that realizing the complete solid-solution reaction during the Na⁺ (de)intercalation is an instructive development direction for designing high-performance cathode materials for SIBs.

CRediT authorship contribution statement

Rui Qi¹: Conceptualization, Investigation, Formal analysis, Visualization, Writing - original draft. Mihai Chu: Conceptualization, Investigation, Formal analysis, Visualization, Writing - original draft. Wenguang Zhao: Investigation. Ziwei Chen: Investigation. Lei Liao: Investigation. Shisheng Zheng: Resources. Xiping Chen: Investigation. Lei Xie: Investigation. Tongchao Liu: Investigation, Resources. Yang Ren: Resources. Lei Jin: Investigation, Resources. Khalil Amine: Resources. Feng Pan: Writing - review & editing, Funding acquisition, Supervision. Yinguo Xiao: Writing - review & editing, Supervision, Project administration, Funding acquisition.

Declaration of Competing Interest

The authors declare that they have no known competing financial interests or personal relationships that could have appeared to influence the work reported in this paper.

Acknowledgements

The research was financially supported by National Key Research and Development Program of China (2020YFA0406203), National Natural Science Foundation of China (No. 52072008 and No. U2032167), Guangdong Basic and Applied Basic Research Foundation (Grant No. 2019A1515012060 and 2019B1515120028). This work gratefully acknowledges support from Clean Vehicles, US-China Clean Energy Research Centre (CERC-CVC2) under US DOE EERE Vehicle Technologies Office. This research used resources of the Advanced Photon Source (11-ID-C), a U.S. Department of Energy (DOE) Office of Science User Facility operated for the DOE Office of Science by Argonne National Laboratory under Contract No. DE-AC02-06CH11357.

Appendix A. Supporting information

Supplementary data associated with this article can be found in the online version at doi:10.1016/j.nanoen.2021.106206.

References

- B. Dunn, H. Kamath, J.-M. Tarascon, Electrical energy storage for the grid: a battery of choices, Science 334 (2011) 928–935.
- [2] C. Delmas, Sodium and sodium-ion batteries: 50 years of research, Adv. Energy Mater. 8 (2018), 1703137.
- [3] C. Vaalma, D. Buchholz, M. Weil, S. Passerini, A cost and resource analysis of sodium-ion batteries, Nat. Rev. Mater. 3 (2018), 18013.
- [4] P.-F. Wang, Y. You, Y.-X. Yin, Y.-G. Guo, Advances in energy, environment and materials science, Adv. Energy Mater. 8 (2018).
- [5] C. Delmas, C. Fouassier, P. Hagenmuller, Structural classification and properties of the layered oxides, Phys. B+C. 99 (1980) 81–85.
- [6] Y. Sun, S. Guo, H. Zhou, Adverse effects of interlayer-gliding in layered transitionmetal oxides on electrochemical sodium-ion storage, Energy Environ. Sci. 12 (2019) 825–840.
- [7] N. Yabuuchi, M. Kajiyama, J. Iwatate, H. Nishikawa, S. Hitomi, R. Okuyama, R. Usui, Y. Yamada, S. Komaba, P2-type Na(x)[Fe(1/2)Mn(1/2)]O2 made from earth-abundant elements for rechargeable Na batteries, Nat. Mater. 11 (2012) 512–517
- [8] M. Chen, Q. Liu, S.-W. Wang, E. Wang, X. Guo, S.-L. Chou, Hybrid supercapacitors: an aqueous zn-ion hybrid supercapacitor with high energy density and ultrastability up to 80 000 cycles, Adv. Energy Mater. 9 (2019), 1970184.
- [9] Y. Fang, Z. Chen, L. Xiao, X. Ai, Y. Cao, H. Yang, Crystal chemistry of vanadiumbearing ellestadite waste forms, Inorg. Chem. 57 (2018) 9122–9132.
- [10] X. Wang, S. Roy, Q. Shi, Y. Li, Y. Zhao, J. Zhang, Progress in and application prospects of advanced and cost-effective iron (Fe)-based cathode materials for sodium-ion batteries, J. Mater. Chem. A 9 (2021) 1938–1969.
- [11] N. Yabuuchi, S. Komaba, Recent research progress on iron- and manganese-based positive electrode materials for rechargeable sodium batteries, Sci. Technol. Adv. Mater. 15 (2014), 043501.
- [12] W.K. Pang, S. Kalluri, V.K. Peterson, N. Sharma, J. Kimpton, B. Johannessen, H. K. Liu, S.X. Dou, Z. Guo, Interplay between electrochemistry and phase evolution of the P2-type Nax(Fe1/2Mn1/2)O2Cathode for use in sodium-ion batteries, Chem. Mater. 27 (2015) 3150–3158.
- [13] W.M. Dose, N. Sharma, J.C. Pramudita, J.A. Kimpton, E. Gonzalo, M.H. Han, T. Rojo, Crystallographic evolution of P2 Na2/3Fe0.4Mn0.6O2electrodes during electrochemical cycling, Chem. Mater. 28 (2016) 6342–6354.
- [14] B. Mortemard de Boisse, D. Carlier, M. Guignard, L. Bourgeois, C. Delmas, P2-Na(x) Mn(1/2)Fe(1/2)O2 phase used as positive electrode in Na batteries: structural changes induced by the electrochemical (de)intercalation process, Inorg. Chem. 53 (2014) 11197–11205
- [15] V. Duffort, E. Talaie, R. Black, L.F. Nazar, Uptake of CO2 in layered P2-Na0.67Mn0.5Fe0.5O2: insertion of carbonate anions, Chem. Mater. 27 (2015) 2515–2524.
- [16] H. Zhu, K.T. Lee, G.T. Hitz, X. Han, Y. Li, J. Wan, S. Lacey, A. Cresce, K. Xu, E. Wachsman, L. Hu, Free-standing Na(2/3)Fe(1/2)Mn(1/2)O(2)@graphene film for a sodium-ion battery cathode, ACS Appl. Mater. Interfaces 6 (2014) 4242–4247.
- [17] S. Kalluri, K.H. Seng, W.K. Pang, Z. Guo, Z. Chen, H.K. Liu, S.X. Dou, Electrospun P2-type Na(2/3)(Fe(1/2)Mn(1/2))O2 hierarchical nanofibers as cathode material for sodium-ion batteries, ACS Appl. Mater. Interfaces 6 (2014) 8953–8958.
- [18] Z. Ding, Y. Liu, Q. Tang, Q. Jiang, J. Lu, Z. Xiao, P. Yao, M. Monasterio, J. Wu, X. Liu, Enhanced electrochemical performance of iron-manganese based cathode by Li doping for sodium-ion batteries, Electrochim. Acta 292 (2018) 871–878.
- [19] L. Yang, X. Li, J. Liu, S. Xiong, X. Ma, P. Liu, J. Bai, W. Xu, Y. Tang, Y.-Y. Hu, M. Liu, H. Chen, Lithium-Doping stabilized high-performance P2-Na0.66Li0.18Fe0.12Mn0.7O2 cathode for sodium ion batteries, J. Am. Chem. Soc. 141 (2019) 6680–6689.
- [20] Y. Li, Z.-Y. Li, K. Sun, Y.-T. Liu, D.-F. Chen, S.-B. Han, L.-F. He, M.-J. Li, X.-L. Liu, M.-M. Wu, Layered Co/Ni-free Mn-rich oxide P2-Na2/3Mn0.8Fe0.1Mg0.102 as high-performance cathode material for sodium-ion batteries, Ionics 26 (2019) 735–743.
- [21] H. Wang, R. Gao, Z. Li, L. Sun, Z. Hu, X. Liu, Different effects of Al substitution for Mn or Fe on the structure and electrochemical properties of Na0.67Mn0.5Fe0.5O2 as a sodium ion battery cathode material, Inorg. Chem. 57 (2018) 5249–5257.
- [22] M. Huon Han, E. Gonzalo, N. Sharma, J. Miguel Lopez del Amo, M. Armand, M. Avdeev, J.J. Saiz Garitaonandia, T. Rojo, High-performance P2-Phase Na2/ 3Mn0.8Fe0.1Ti0.1O2cathode material for ambient-temperature sodium-ion batteries, Chem. Mater. 28 (2016) 106–116.
- [23] M. Zarrabeitia, E. Gonzalo, M. Pasqualini, M. Ciambezi, O. Lakuntza, F. Nobili, A. Trapananti, A. Di Cicco, G. Aquilanti, N.A. Katcho, J.M. López del Amo, J. Carrasco, M.Á. Muñoz-Márquez, T. Rojo, Unraveling the role of Ti in the stability of positive layered oxide electrodes for rechargeable Na-ion batteries, J. Mater. Chem. A 7 (2019) 14169–14179.
- [24] D. Yuan, X. Hu, J. Qian, F. Pei, F. Wu, R. Mao, X. Ai, H. Yang, Y. Cao, Thermal stability of Mn2+ ion luminescence in Mn-doped core-shell quantum dots, Nanoscale 6 (2014) 300–307.
- [25] L. Liu, X. Li, S.-H. Bo, Y. Wang, H. Chen, N. Twu, D. Wu, G. Ceder, Lithium batteries: highly nitridated graphene-Li2S cathodes with stable modulated cycles, Adv. Energy Mater. 5 (2015).

- [26] Y.H. Jung, A.S. Christiansen, R.E. Johnsen, P. Norby, D.K. Kim, In situ x-ray diffraction studies on structural changes of a p2 layered material during electrochemical desodiation/sodiation, Adv. Funct. Mater. 25 (2015) 3227–3237.
- [27] S. Xu, J. Wu, E. Hu, Q. Li, J. Zhang, Y. Wang, E. Stavitski, L. Jiang, X. Rong, X. Yu, W. Yang, X.-Q. Yang, L. Chen, Y.-S. Hu, Suppressing the voltage decay of low-cost P2-type iron-based cathode materials for sodium-ion batteries, J. Mater. Chem. A 6 (2018) 20795–20803.
- [28] Q. Shen, X. Zhao, Y. Liu, Y. Li, J. Zhang, N. Zhang, C. Yang, J. Chen, Dual-strategy of cation-doping and nanoengineering enables fast and stable sodium-ion storage in a novel fe/mn-based layered oxide cathode, Adv. Sci. (Weinh.) 7 (2020), 2002199.
- [29] U. Garg, W. Rexhausen, N. Smith, J. Harris, D. Qu, P. Guptasarma, Pleural effusions associated with spinal tuberculosis, J. Emerg. Med. 57 (2019) 105–113.
- [30] Y. Li, Z. Yang, S. Xu, L. Mu, L. Gu, Y.S. Hu, H. Li, L. Chen, Air-stable copper-based P2-Na7/9Cu2/9Fe1/9Mn2/3O2 as a new positive electrode material for sodiumion batteries, Adv. Sci. (Weinh.) 2 (2015), 1500031.
- [31] D. Kundu, E. Talaie, V. Duffort, L.F. Nazar, The emerging chemistry of sodium ion batteries for electrochemical energy storage, Angew. Chem. Int Ed. Engl. 54 (2015) 3431–3448.
- [32] X. Gao, J. Chen, H. Liu, S. Yin, Y. Tian, X. Cao, G. Zou, H. Hou, W. Wei, L. Chen, X. Ji, The hierarchical layered microsphere of BiOlxBr1-x solid solution decorated with N-doped CQDs with enhanced visible light photocatalytic oxidation pollutants, Chem. Eng. J. 406 (2021), 127155.
- [33] Y. Li, M. Chen, B. Liu, Y. Zhang, X. Liang, X. Xia, Characterization of the valence and conduction band levels ofn= 1 2d perovskites: a combined experimental and theoretical investigation, Adv. Energy Mater. 10 (2020), 2000390.
- [34] J. Deng, W.-B. Luo, X. Lu, Q. Yao, Z. Wang, H.-K. Liu, H. Zhou, S.-X. Dou, Biochemical changes of Coregonus peled myofibrillar proteins isolates as affected by HRGS oxidation system, J. Food Biochem 43 (2019), 12710.
- [35] Y. Xiao, Y.-F. Zhu, H.-R. Yao, P.-F. Wang, X.-D. Zhang, H. Li, X. Yang, L. Gu, Y.-C. Li, T. Wang, Y.-X. Yin, X.-D. Guo, B.-H. Zhong, Y.-G. Guo, A stable layered oxide cathode material for high-performance sodium-ion battery, Adv. Energy Mater. 9 (2019), 1803978.
- [36] C. Zhao, F. Ding, Y. Lu, L. Chen, Y.S. Hu, High-entropy layered oxide cathodes for sodium-ion batteries, Angew. Chem. Int. Ed. 59 (2020) 264–269.
- [37] J. Xu, D.H. Lee, R.J. Clément, X. Yu, M. Leskes, A.J. Pell, G. Pintacuda, X.-Q. Yang, C.P. Grey, Y.S. Meng, Identifying the critical role of Li substitution in P2–Nax [LiyNizMn1–y–z]O2(0 < x,y,z < 1) intercalation cathode materials for high-energy Na-ion batteries, Chem. Mater. 26 (2014) 1260–1269.</p>
- [38] T. Jin, P.F. Wang, Q.C. Wang, K. Zhu, T. Deng, J. Zhang, W. Zhang, X.Q. Yang, L. Jiao, C. Wang, Realizing complete solid-solution reaction in high sodium content P2-Type cathode for high-performance sodium-ion batteries, Angew. Chem. Int Ed. Engl. 59 (2020) 14511–14516.
- [39] Y. You, S. Xin, H.Y. Asl, W. Li, P.-F. Wang, Y.-G. Guo, A. Manthiram, Insights into the improved high-voltage performance of Li-incorporated layered oxide cathodes for sodium-ion batteries, Chem 4 (2018) 2124–2139.
- [40] C. Zhao, Z. Yao, Q. Wang, H. Li, J. Wang, M. Liu, S. Ganapathy, Y. Lu, J. Cabana, B. Li, X. Bai, A. Aspuru-Guzik, M. Wagemaker, L. Chen, Y.S. Hu, Revealing high Na-Content P2-type layered oxides as advanced sodium-ion cathodes, J. Am. Chem. Soc. 142 (2020) 5742–5750.
- [41] C.W. Mason, F. Lange, K. Saravanan, F. Lin, D. Nordlund, Beyond divalent copper: a redox couple for sodium ion battery cathode materials, ECS Electrochem. Lett. 4 (2015) A41–A44.
- [42] Z. Yan, L. Tang, Y. Huang, W. Hua, Y. Wang, R. Liu, Q. Gu, S. Indris, S.L. Chou, Y. Huang, M. Wu, S.X. Dou, A hydrostable cathode material based on the layered P2@P3 composite that shows redox behavior for copper in high-rate and long-cycling sodium-ion batteries, Angew. Chem. Int Ed. Engl. 58 (2019) 1412–1416.
- [43] X. Zheng, P. Li, H. Zhu, K. Rui, G. Zhao, J. Shu, X. Xu, W. Sun, S.X. Dou, New insights into understanding the exceptional electrochemical performance of P2type manganese-based layered oxide cathode for sodium ion batteries, Energy Storage Mater. 15 (2018) 257–265.
- [44] E. Talaie, V. Duffort, H.L. Smith, B. Fultz, L.F. Nazar, Structure of the high voltage phase of layered P2-Na2/3-z[Mn1/2Fe1/2]O2and the positive effect of Ni substitution on its stability, Energy Environ. Sci. 8 (2015) 2512–2523.
- [45] J.W. Somerville, A. Sobkowiak, N. Tapia-Ruiz, J. Billaud, J.G. Lozano, R.A. House, L.C. Gallington, T. Ericsson, L. Häggström, M.R. Roberts, U. Maitra, P.G. Bruce, Nature of the "Z"-phase in layered Na-ion battery cathodes, Energy Environ. Sci. 12 (2019) 2223–2232.
- [46] S. Guo, Y. Sun, P. Liu, J. Yi, P. He, X. Zhang, Y. Zhu, R. Senga, K. Suenaga, M. Chen, H. Zhou, Synthesis, photophysical and electrochemical properties of a blue emitter with binaphthalene and carbazole units, Spectrochim. Acta A Mol. Biomol. Spectrosc. 201 (2018) 376–381.
- [47] Y. Cao, Q. Zhang, Y. Wei, Y. Guo, Z. Zhang, W. Huang, K. Yang, W. Chen, T. Zhai, H. Li, Y. Cui, A water stable, near-zero-strain O3-layered titanium-based anode for long cycle sodium-ion battery, Adv. Funct. Mater. 30 (2020), 1907023.
- [48] Y. Wang, L. Wang, H. Zhu, J. Chu, Y. Fang, L. Wu, L. Huang, Y. Ren, C.J. Sun, Q. Liu, X. Ai, H. Yang, Y. Cao, 3D printing of a biocompatible double network elastomer with digital control of mechanical properties, Adv. Funct. Mater. 30 (2020).
- [49] J. Xu, Z. Han, K. Jiang, P. Bai, Y. Liang, X. Zhang, P. Wang, S. Guo, H. Zhou, Suppressing cation migration and reducing particle cracks in a layered fe-based cathode for advanced sodium-ion batteries, Small 16 (2020), 1904388.
- [50] P. Yan, J. Zheng, M. Gu, J. Xiao, J.G. Zhang, C.M. Wang, Intragranular cracking as a critical barrier for high-voltage usage of layer-structured cathode for lithium-ion batteries, Nat. Commun. 8 (2017), 14101.

- [51] K. Wang, P. Yan, M. Sui, Phase transition induced cracking plaguing layered cathode for sodium-ion battery, Nano Energy 54 (2018) 148–155.
- [52] J. Song, K. Wang, J. Zheng, M.H. Engelhard, B. Xiao, E. Hu, Z. Zhu, C. Wang, M. Sui, Y. Lin, D. Reed, V.L. Sprenkle, P. Yan, X. Li, Controlling surface phase transition and chemical reactivity of O3-layered metal oxide cathodes for high-performance Na-ion batteries, ACS Energy Lett. 5 (2020) 1718–1725.
- [53] L.J. Krause, V.L. Chevrier, L.D. Jensen, T. Brandt, The Effect of Carbon Dioxide on the Cycle Life and Electrolyte Stability of Li-Ion Full Cells Containing Silicon Alloy, J. Electrochem. Soc. 164 (2017) A2527–A2533.
- [54] T. Liu, A. Dai, J. Lu, Y. Yuan, Y. Xiao, L. Yu, M. Li, J. Gim, L. Ma, J. Liu, C. Zhan, L. Li, J. Zheng, Y. Ren, T. Wu, R. Shahbazian-Yassar, J. Wen, F. Pan, K. Amine, Correlation between manganese dissolution and dynamic phase stability in spinel-based lithium-ion battery, Nat. Commun. 10 (2019), 4721.
- [55] J. Billaud, G. Singh, A.R. Armstrong, E. Gonzalo, V. Roddatis, M. Armand, T. Rojo, P.G. Bruce, Na0.67Mn1-xMgxO2(0 \leq x \leq 0.2): a high capacity cathode for sodium-ion batteries, Energy Environ. Sci. 7 (2014) 1387–1391.
- [56] E. Gonzalo, N. Ortiz-Vitoriano, N.E. Drewett, B. Acebedo, J.M. López del Amo, F. J. Bonilla, T. Rojo, P2 manganese rich sodium layered oxides: rational stoichiometries for enhanced performance, J. Power Sources 401 (2018) 117–125.
- [57] J. Xia, R. Petibon, A. Xiao, W.M. Lamanna, J.R. Dahn, Inhibition of SUMO-specific protease 1 induces apoptosis of astroglioma cells by regulating NF-κB/Akt pathways, Gene 595 (2016) 175–179.
- [58] K.-J. Park, J.-Y. Hwang, H.-H. Ryu, F. Maglia, S.-J. Kim, P. Lamp, C.S. Yoon, Y.-K. Sun, Degradation mechanism of Ni-enriched NCA cathode for lithium batteries: are microcracks really critical, ACS Energy Lett. 4 (2019) 1394–1400.
- [59] W. Zuo, J. Qiu, X. Liu, F. Ren, H. Liu, H. He, C. Luo, J. Li, G.F. Ortiz, H. Duan, J. Liu, M.-S. Wang, Y. Li, R. Fu, Y. Yang, Nat. Commun. 11 (2020).
- [60] H.-R. Yao, P.-F. Wang, Y. Gong, J. Zhang, X. Yu, L. Gu, C. OuYang, Y.-X. Yin, E. Hu, X.-Q. Yang, E. Stavitski, Y.-G. Guo, L.-J. Wan, Designing air-stable O3-type cathode materials by combined structure modulation for na-ion batteries, J. Am. Chem. Soc. 139 (2017) 8440–8443.



Rui Qi is currently pursuing his M.Sc. degree under the supervision of Prof. Feng Pan at Peking University Shenzhen Graduate School, China. He received his B.Eng. from Central South University in 2018. His research interests mainly focus on investigating the relation between the structure of cathode materials for Li- and Na-ion batteries and their electrochemical behavior.



Mihai Chu received his B.Eng. degree from the School of Optical and Electronic Information at Huazhong University of Science and Technology in 2017. He is currently pursuing his master degree in the School of Advanced Materials, Peking University under the supervision of Prof. Yinguo Xiao. His research interests mainly focus on the synthesis of cathode materials for Li- and Na-ion batteries and their structural characterization based on X-ray and neutron diffraction methods.



Wenguang Zhao is an engineer in the School of Advanced Materials, Peking University Shenzhen Graduate School, China. He has over 10 years' experience in material characterization using wide range of analytical tools including XRD, XPS, SEM and TEM. His research interests mainly focus on the Ex/in-situ TEM and Ex/in-situ XRD characterization of battery materials.

R. Qi et al. Nano Energy 88 (2021) 106206



Ziwei Chen received his bachelor's degree of engineering from the School of Material Science and Chemical engineering at Ningbo University in 2019. He is currently pursuing his master degree in the School of Advanced Materials, Peking University under the supervision of Prof. Yinguo Xiao. His research interest is the synthesis of layered cathode materials and structure characterization based on X-ray and neutron diffraction



Dr. Tongchao Liu currently works as a Postdoctoral Appointee at Argonne National Laboratory. He obtains his Ph.D. degree from Peking University in 2019. His research interests are focused on the interface of electrochemistry, cathode materials and materials characterization, in particular, concentration gradient cathode design and fundamental understanding of failure chemistries through in-situ synchrotron-based X-ray



Lei Liao received his B.S. degree from School of Materials Science and Engineering, Central South University in 2018. Liao is now pursuing his Ph.D. degree under the supervision of Prof. Xuedong Bai at Institute of Physics, Chinese Academy of Sciences. His research focuses on in-situ aberration-corrected STEM imaging of polarization switching dynamic in ferroelectrics.



Dr. Yang Ren received his M.S. degree in condensed matter physics from the Institute of Physics, Chinese Academy of Science, China, and his Ph.D. degree in Chemical Physics from the University of Groningen, The Netherlands. He is currently a senior physicist and lead beamline scientist at the Advanced Photon Source, Argonne National Laboratory, USA. His research interests focus on the structure-property studies of materials by utilizing synchrotron X-ray and neutron scattering and other techniques. His research activities include the investigation of phase transition, correlated electron systems, engineering materials, nanoparticles and nanocomposites, energy storage and conversion materials.



Shisheng Zheng received his BE degree in the College of Energy at the Xiamen University. He is currently a Ph. D. candidate in School of Advanced Material under the supervision of Prof. Feng Pan at the Peking University. His current research focuses on computational studies of catalyst materials and battery materials.



conditions.

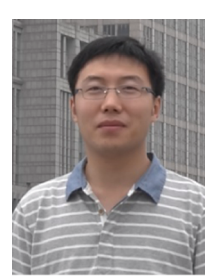
Dr. Lei Jin received his Ph.D. degree from School of Physics and Technology and Center for Electron Microscopy, Wuhan University, China in 2008. From 2005-2006, he acted as a technical assistant (exchange student) in Department of Electrical and Electronic Engineering, The University of Hong Kong, Hong Kong, China. After working shortly in Wuhan University in 2009, he was a postdoctoral researcher in the Ernst Ruska-Centre for Microscopy and Spectroscopy with Electrons, Forschungszentrum Jülich GmbH, Germany from 2009 to 2016. Since 2017, he was promoted as a tenured scientist. His research interests include quantitative highresolution transmission electron microscopy and spectroscopy, structural defects in functional oxides and related behavior under working



Xiping Chen received his M.S. degree from China Academy of Engineering Physics, China in 2012. In 2000, he joined the Institute of nuclear physics and chemistry of the Chinese Academy of Engineering Physics and served as an associate researcher in 2012. His research interests are on research and development neutron scattering spectrometer technology.



Dr. Khalil Amine is an Argonne Distinguished Fellow and the leader of the Advanced Battery Technology team at Argonne National Laboratory, where he is responsible for directing the research and development of advanced materials and battery systems for HEV, PHEV, EV, and satellite applications. He is an adjunct professor at Stanford University. Among his many awards, Dr. Amine is the 2019 reception of the prestigious Global Energy Prize. He is a six-time recipient of the R&D 100 Award, which is considered as the Oscar of technology and innovation. He is an ECS fellow, and associate editor of the journal of Nano-Energy.



Dr. Lei Xie received his Ph.D. degree from China Academy of Engineering Physics, China in 2019. In 2004, he joined Institute of Nuclear Physics and Chemistry, China Academy of Engineering Physics, China as an assistant researcher. He has been engaged in research and development of neutron diffraction techniques and applications.



Dr. Feng Pan, founding Dean of School of Advanced Materials, Peking University Shenzhen Graduate School, got B.S. from Dept. Chemistry, Peking University in 1985 and Ph.D. from Dept. of P&A Chemistry, University of Strathclyde, Glasgow, UK, with "Patrick D. Ritchie Prize" for the best Ph.D. in 1994. With more than a decade experience in large international incorporations, Prof. Pan has been engaged in fundamental research and product development of novel optoelectronic and energy storage materials and devices. As Chief Scientist, Prof. Pan led eight entities in Shenzhen to win 150 million RMB grant for the national new energy vehicles (power battery) innovation project since 2013.

R. Qi et al. Nano Energy 88 (2021) 106206



Dr. Yinguo Xiao received his Ph.D. degree from Institute of Physics, Chinese Academy of Sciences, China in 2006. He was a postdoctoral fellow from 2007 to 2009 and a research scientist from 2009 to 2014 at Juelich Research Centre (Forschungszentrum Jülich), Germany. He became a tenured staff scientist in Juelich Research Centre since 2015. In 2017, he joined Peking University Shenzhen Graduate School, China as an associate professor. His research interests are on research and development of new materials for energy conversion and storage, and characterization of complex materials using X-ray and neutron scattering techniques.